J Mater Sci (2007) 42:9137–9144
DOI 10.1007/s10853-007-1931-0

Studies on electrodeposition and corrosion behaviour of a Ni–W–Co amorphous alloy

Renato Alexandre C. Santana · Ana Regina N. Campos · Emanuelle A. Medeiros · Aldrighi Luiz M. Oliveira · Liana Maria F. Silva · Shiva Prasad

Received: 29 November 2006 / Accepted: 11 June 2007 / Published online: 28 July 2007

Abstract A ternary alloy Ni–W–Co was electrodeposited and operational parameters in relation to its corrosion resistance and deposition efficiency were optimized. A 2^2 full factorial design was successfully employed for experimental design analysis of the results. By means of response surface analysis, the statistical model identified the following operating conditions for obtaining corrosion resistant alloy: 60 mA/cm^2 current density, 70 °C temperature, 20 rpm cathode rotation and 8.0 pH. The alloy was deposited at 36% current efficiency, with an average composition of 70% Ni, 8% Co, 22% W and traces of boron and with E_{corr} –0.508 V and R_p 4.56×10^4 Ohm. The deposit obtained under these conditions had an amorphous character and showed good adherence, high corrosion resistance and presence of nodules on its surface. Electrochemical corrosion tests verified that the Ni–W–Co alloy had better corrosion resistance than similarly electrodeposited Co–W amorphous alloy.

Introduction

Tungsten alloys exhibit high corrosion resistance and good mechanical properties, which make them suitable for many engineering applications. Recently they have been deposited as barrier layers used for ultralarge-scale. The Ni–Co alloys were the first to be utilized in the production of magnetic-film memories just because of their desirable soft magnetic properties, and were widely used later. They also found application in surface micromachining. The introduction of tungsten to the alloys of this type improved their durability, hardness and resistance to high temperatures [1]. The interest in electrodeposition of tungsten alloys has increased in recent years due to their unique combination of tribological, magnetic, electrical and corrosion resistance properties. It has been found that the alloys with tungsten can be deposited in the amorphous form [2]. The presence of tungsten in the amorphous alloys apparently increased the corrosion resistance of these and other similar materials [3, 4]. Applications of the tungsten alloys include their use as electrodes to promote the hydrogen evolution [5].

Electrodeposition of tungsten in the pure state has not yet been successful from either aqueous or organic solutions. But no experimental difficulty is experienced in codepositing tungsten with the group 8 metals [6]. Several authors have investigated the process of electrodeposition of tungsten with iron group metals in aqueous solutions [7–10].

Conventional and classical methods of studying a process by maintaining other factors involved at an unspecified constant level does not depict the combined effect of all the factors involved. This method is also time consuming and requires large number of experiments to determine optimum levels, which are unreliable. These limitations of a classical method can be eliminated by optimizing all the affecting parameters collectively by statistical experimental design such as Response Surface Methodology (RSM) [11]. The experimental factorial design investigations present several advantages over such univariate methods. Factors are varied simultaneously rather than one-at-a-time permitting observation of synergic and antagonistic interactions involving the factors.

R. A. C. Santana · A. R. N. Campos · E. A. Medeiros · A. L. M. Oliveira · L. M. F. Silva · S. Prasad (✉)
Department of Chemical Engineering, Universidade Federal de Campina Grande, Post Box 10108, Campina Grande, Paraiba 58109-970, Brazil
e-mail: prasad@deq.ufcg.edu.br

Univariate methods are incapable of measuring these interactions and for this reason are not effective optimization techniques. RSM is a collection of mathematical and statistical techniques useful for developing, improving and optimizing processes and can be used to evaluate the relative significance of several affecting factors even in the presence of complex interactions. The main objective of RSM is to determine the optimum operational conditions for the system or to determine a region that satisfies the operating specifications [12].

With the objective of improving the characteristics of Co–W alloy that possesses interesting catalytic properties but low corrosion resistance, nickel has been added to the bath composition of this alloy so that to improve its anticorrosive properties. No any reference could be traced out in the literature for electrodeposition of this ternary alloy except the results presented in 1980 by Singh et al. [13]. The results of studies to optimize operational parameters namely current density and bath temperature for electrodeposition of corrosion resistant Ni–W–Co amorphous alloy are reported here. The interaction between the parameters was studied and optimized using response surface methodology.

Experimental

The electrochemical bath was prepared using analytical grade chemicals and double distilled, deionized water. The bath used for electrodeposition of the alloy Ni–W–Co contained 0.0370 M nickel sulfate, 0.010 M cobalt sulfate, 0.0310 M sodium tungstate, 0.0728 M boron phosphate, 0.0875 M sodium citrate and 0.017 g/L 1-Na-dodecylsulfate and ammonium hydroxide for initial adjustment of pH for 8.0. Ammonium hydroxide is preferred in comparison to NaOH for pH adjustment since it helps in stabilizing the bath by its complexing action. The bath pH was adjusted during the deposition process using either ammonium hydroxide or sulfuric acid. The bath used in this study was developed from bath composition of the alloy Ni–W [14]. The electrodeposition process was usually performed for a period of 1 h.

Prior to the coating deposition, the substrate was polished up to 1200 grit surface finish using 400, 600 and 1200 grits, respectively. The electrodeposition was performed under galvanostatic control on rotating rectangular plane copper foil of 0.5 mm thickness and of about 8 cm^2 surface area acting as cathode which was placed inside a cylindrical platinum gauze anode. The substrate was inserted in the cell as a cathode and fixed with an RDE electrode for the agitation. All specimens were subjected to a series of cleaning stages and finally rinsed in dilute 10% H_2SO_4 to remove any residual alkali [14].

A potentiostat/galvanostat (Autolab PGSTATE 30) was used to apply a known current density to the cathode. An MTA KUTESZ MD2 thermostat controlled the temperature of the bath and a rotating electrode EG&G PARC 616 (cathode rotation), was used to control mechanical agitation. The Faradaic efficiency was calculated from the charge passed and the weight gained. The alloy composition was taken into account when calculating the deposition efficiency.

A complete factorial design of two levels and two factors (2^2) was used [15], totaling four experiments plus three experiments in the center point, for a quantitative evaluation of the influence of current density and bath temperature on the alloy deposition efficiency and corrosion resistance (polarization resistance). All the experiments were performed in triplicate. Table 1 shows the levels of the factors used, as well as their experimental design codes. Each independent factor was investigated at a high (+1) and a low (–1) level. The center point (0) replicates were chosen to verify any change in the estimation procedure, as a measure of precision property. Those variables having a major effect on deposition efficiency and corrosion resistance were identified on the basis of confidence levels above 95% ($p < 0.05$).

The potentiodynamic linear polarization (PLP) and electrochemical impedance spectroscopy (EIS) studies were performed by using a potentiostat (Autolab PGSTATE 30) for corrosion analysis. A saturated calomel electrode (Hg/Hg_2Cl_2) and Pt foil were used as reference and auxiliary electrodes, respectively. The PLP curves were obtained with a sweep rate of 1 mV/s in a potential range –1 to 2 V and the impedance spectroscopy experiments were carried out at selected potentials from the PLP curves with a frequency interval of 1 kHz to 0.004 Hz. About 60 min waiting period was used for stabilization prior to starting the tests of PLP and EIS. All the electrochemical corrosion tests were conducted in aqueous 0.1 M NaCl at room temperature and in ambient atmosphere.

Characterization of the amorphous structure of the alloy was determined by X-ray diffraction (XRD), using SHIMADZU XRD-6000 Diffractometer, with Cu Kα radiation, a step size of 0.02° and a dwell time of 1s.

The surface morphology and cross section analysis of the amorphous electrodeposited layers were examined by scanning electron microscopy (SEM) using a Philips

Table 1 Actual and coded levels of factors studied

Factors	Code		
	–1	0	+1
Current density/mA/cm^2	20	40	60
Temperature/°C	30	50	70

XL-30 scanning electron microscope. The composition of the alloy was determined by energy dispersive X-ray analysis (EDX) using a Link Analytical QX-2000 attached to the SEM apparatus.

Results and discussion

Factorial matrix used to optimize the operational parameters for electrodeposition and the results of the electrodeposition efficiency, alloy composition and corrosion resistance (polarization resistance) are presented in Table 2.

The results were subjected to multiple non-linear regression analysis to obtain coefficients for each of the parameters. Estimates of the coefficients with levels higher than 95% ($p < 0.05$) were included in the final model. Deposition efficiency (Eff.) and polarization resistance (R_p) can thus be expressed as functions of the independent factors by the linear mathematical model represented by Eqs. 1 and 2 respectively, where (I) is current density, (t) is temperature and ($I * t$) is interaction between current density and temperature. Taking into account only the significant effects, the following equations correspond to the surface response shown in Figs. 1 and 2. The final response equations, where the significant terms showed in bold, are given as follows:

$$\text{Eff. } (\%) = \mathbf{40.57} + 2.33\,I - \mathbf{2.57}\,t - \mathbf{2.68}\,I * t \quad (1)$$

$$R_p \text{ (Ohm)} = \mathbf{23435} + \mathbf{4625}\,I + \mathbf{12625}\,t + \mathbf{5175}\,I * t \quad (2)$$

Analysis of variance (ANOVA) showed that these models were significant at a 95% confidence level. The fit of the models was also expressed by the determination coefficient (R^2) equal to 0.92313 and 0.99902 for Eff. and R_p, respectively. This means that regression model provides an excellent explanation of the relationship between the independent variables (factors) and the response (Eff. and R_p). The associated p-value for the model is lower than 0.05 (i.e., $\alpha = 0.05$, or 95% confidence) indicates that the

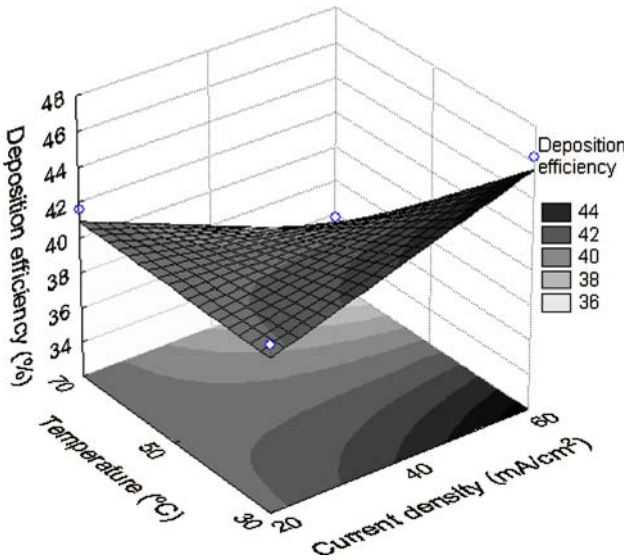

Fig. 1 Fitted surface of influence of current density versus temperature in relation to deposition efficiency of the alloy, using a bath pH of 8.0 and rotation rate at 20 rpm

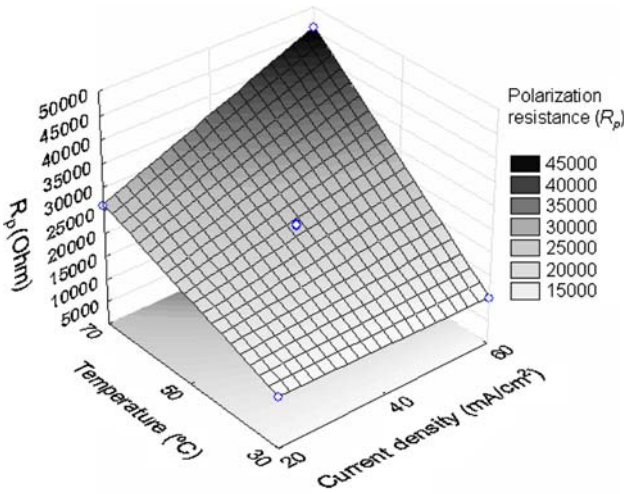

Fig. 2 Fitted surface of influence of current density versus temperature in relation to polarization resistance of the alloy, using a bath pH of 8.0 and rotation rate at 20 rpm

Table 2 Electrodepostion efficiency, corrosion resistance and deposit composition as shown by the factorial matrix

Runs	Current density	Temp.	R_p/Ohm	Co/≈wt.%	Ni/≈wt.%	W/≈wt.%	Deposition efficiency/%
1	–1	–1	11100	07.93	70.45	21.62	41.396
2	–1	+1	26000	17.46	56.46	26.29	41.614
3	+1	–1	10000	18.42	45.86	35.72	46.306
4	+1	+1	45600	12.39	46.29	41.32	35.772
5	0	0	24100	9.58	55.49	34.93	38.822
6	0	0	23500	11.02	54.41	34.47	38.499
7	0	0	23750	10.32	54.98	34.83	38.589

model is considered to be statistically significant, justifying the use of a linear model for the statistical analysis. Statistical evaluation of the model was done by the Fisher's test for analysis of variance whose results are shown in Tables 3 and 4. The results of the ANOVA for purity degree, listed in Table 3, demonstrate that the statistical model is significant at the 95% confidence level ($p < 0.05$) [16]. Equation 1 fitted the experimental data with an acceptable determination coefficient (R^2 0.92313).

The results of the ANOVA for purity degree, listed in Table 4, demonstrate that the statistical model is significant at the 95% confidence level ($p < 0.05$). Equation 2 fitted the experimental data with an acceptable determination coefficient (R^2 0.99902).

Effect of current density

The effect of current density on process efficiency was studied in the range 20–60 mA/cm^2. Regression analysis of the experimental data showed that current density was statically insignificant operational factor in the electrodeposition process at a 95% confidence level (Eq. 1). From this observation and the F test results it can be concluded that the statistical model used in these experiments was representative and reproducible (Tables 3 and 4). In contrast, the interaction of current density and temperature was statistically significant showing a synergic interaction among these factors on the electrodeposition process [12].

The highest value for the deposition efficiency, approximately 46%, was obtained by using a high current density 60 mA/cm^2. From the experimental data (Table 2) it was observed that an increase in current density increased deposition efficiency (Fig. 1) as well as corrosion resistance (Fig. 2) [17]. Besides this, the effect of increase in current density on corrosion resistance was statistically significant (Eq. 2). The optimal operating conditions corresponding to corrosion resistance (i.e., polarization resistance) were obtained with a current density 60 mA/cm^2. This was associated with a high tungsten wt.% (Table 2) when compared with the deposits obtained with a current density 20 mA/cm^2.

As shown in Table 2, the low current densities favour the deposition of Ni where as the high current densities favour the deposition of W, as also reported by Eliaz et al. [8]. Yamasaki et al. [18] also observed a significant increase in tungsten content with increasing current density in citrate bath.

Effect of temperature

Temperature is another important factor in the operation of tungsten alloy plating baths. An increase in temperature usually decreases polarization, increases the concentration of metal in the cathode diffusion layer and may affect the cathode current efficiency for metal deposition, particularly those deposited from complex ions. The effect of bath temperature on the process efficiency was studied in the temperature range 30–70 °C. From Eq. 1, it can be confirmed that the temperature change has the most statistically significant effect on the process efficiency at the 95% level.

Table 3 Results of ANOVA of deposit efficiency

Source	Sum of squares	Degrees of freedom	Mean square	F	p
(1) Current density	26.605	1	26.605	17.201	0.025
(2) Temperature	0.217	1	0.217	0.140	0.733
Interaction 1 and 2	28.901	1	28.901	18.686	0.023
Residual error	4.640	3	1.547		
Lack of fit	4.584	1			
Total	65.002	6			

Table 4 Results of ANOVA of corrosion resistance

Source	Sum of squares	Degrees of freedom	Mean square	F	p
(1) Current density	85562500	1	85562500	941.97	0.00106
(2) Temperature	637562500	1	637562500	7019.07	0.00014
Interaction 1 and 2	107122500	1	107122500	1179.33	0.00085
Residual error	634405	1	634405		
Lack of fit	181667	2			
Total	831063571	6			

Figure 1 shows the estimated response surface for current efficiency in relation to the design parameters of current density and temperature. It can be seen from this figure that the current efficiency tends to increase with decrease in temperature to 30 °C.

The effect of current density and temperature on corrosion resistance is shown in Fig. 2. Bath temperature showed a statistically significant effect on corrosion resistance of the deposit (Eq. 2). The statistical results obtained in this study suggest that the increase in bath temperature increased corrosion resistance of the deposit.

Appearance of the deposit

Scanning electron microscope (SEM) analysis showed that the alloy Ni–W–Co (Fig. 3) deposited on the copper substrate presented a substantial decrease in number of microcracks in comparison to those on the deposits of Co–W alloy (Fig. 4). The deposit of Ni–W–Co was nodular. With increase in current density from the level of 40 mA/cm^2 the number of nodules was increased and their size decreased, besides the formation of agglomerates of the nodules (Fig. 5). The deposit of Co–W showed microcracks on its surface, which reached down to the copper substrate [14].

The Ni–W–Co deposit also showed good adherence (to usual mechanical method) and luster, with an average thickness of 22 μm after 1 h of electrodeposition. The composition of the electro-deposited alloy was obtained with the help of EDX (Table 2).

The amorphous character of the as-deposited alloys is confirmed by XRD patterns in which there is only a broad feature at around $2\theta = 44^{o}$; a single broad peak confirmed the amorphous structure of the alloy (Fig. 6). Boron was added to the bath in the form of boron phosphate, which was co-deposited in the alloy, producing an amorphous structure, and consequently the interesting properties, such

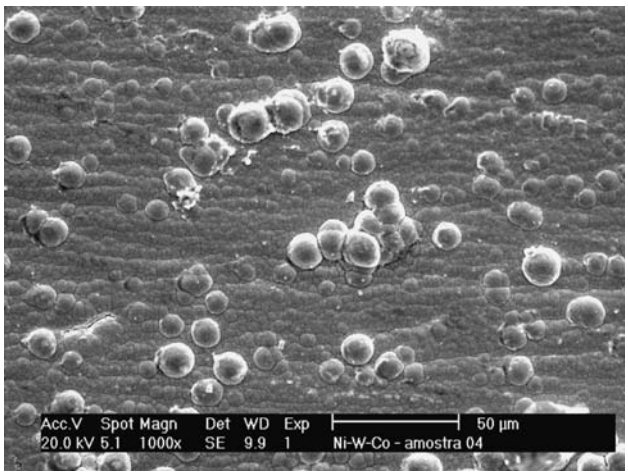

Fig. 3 SEM micrographs of the Ni–W–Co alloy surface, with 1000× amplification (current density 20 mA/cm^2, temperature 70 °C, pH 8.0 and rotation rate 20 rpm)

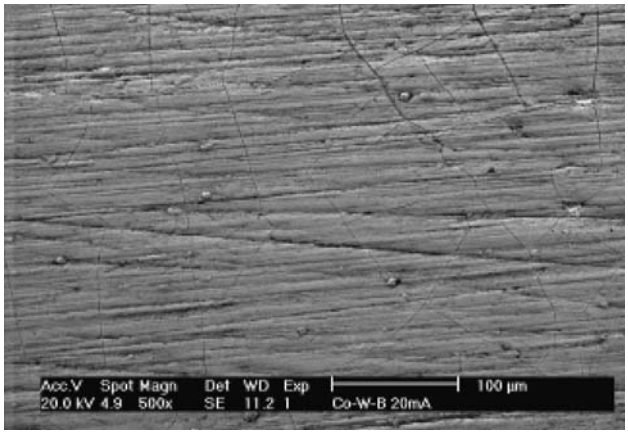

Fig. 4 SEM micrographs of the Co–W alloy surface, with 500× amplification (current density 20 mA/cm^2, temperature 70 °C, pH 9.5 and rotation rate 90 rpm)

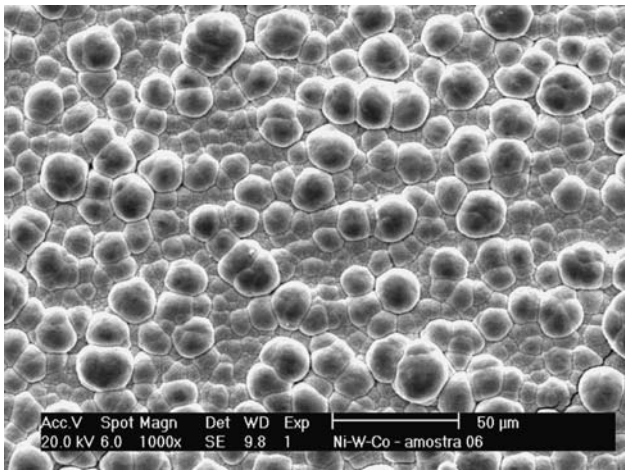

Fig. 5 SEM micrographs of the Ni–W–Co alloy surface, with 1000× amplification (current density 60 mA/cm^2, temperature 70 °C, pH 8.0 and rotation rate 20 rpm)

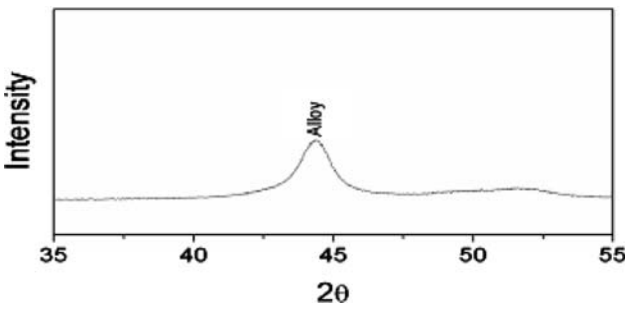

Fig. 6 X-ray diffraction patterns of as-electrodeposited Ni–W–Co alloy

as a high level of hardness [19]. Similar behaviour was observed by Wonterghem et al. [20], Qiao et al. [21] and Dai et al. [22]. According to Einati et al. the addition of boron favours the formation of amorphous structure besides increase in resistance of thin films, improving the stability of these films against the air oxidation [23].

Corrosion resistance

Corrosion characterization of the alloy Ni–W–Co deposited on copper substrate with the optimized operational parameters was realized by linear polarization curves. Figure 7 shows potentiodynamic polarization curves obtained for the alloys Co–W and Ni–W–Co deposited under optimal conditions for corrosion resistance in 0.1 M NaCl. It can be observed that the electrodeposits containing Ni–W–Co had corrosion potentials ≈172 mV more positive than that of the electrodeposition containing Co–W. Corrosion resistance of Ni–W–Co alloy increased with increase in percentage of tungsten in the deposit (Table 2). The Co–W alloy showed micro-cracks on its surface favouring the corrosion attack. The dissolution process of both the alloys increased with the increase in potential; however the Ni–W–Co deposit showed greater resistance and higher stability during the corrosive process. The analysis reveals that Ni–W–Co alloy is more corrosion resistant than the Co–W alloy (Table 5).

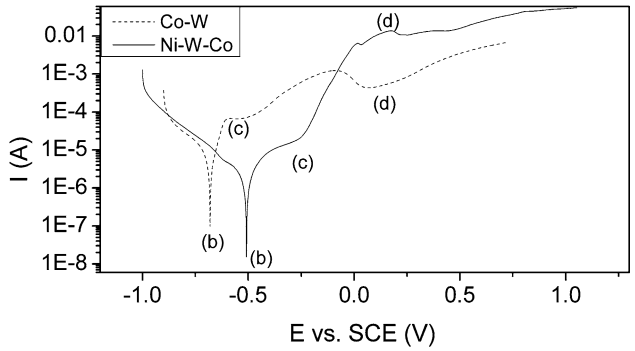

Fig. 7 Anodic polarization curve of Co–W alloy (current density 20 mA/cm^2, temperature 70 °C, pH 9.5 and rotation rate 90 rpm); and anodic polarization curve of Ni–W–Co alloy (current density 60 mA/cm^2, temperature 70 °C, pH 8.0 and rotation rate 20 rpm)

Table 5 Corrosion data obtained from potentiodynamic polarization curves

Corrosion data	Ni–Co–W	Co–W
E_{corr}/V	–0.508	–0.680
R_p/Ohm	4.56×10^4	1.20×10^3

Electrochemical impedance spectroscopy measurements were carried out to obtain detailed information about the corrosion resistance behaviour of Ni–W–Co and Co–W alloys. The impedance measurements were performed at open circuit potential (a) and also in the regions b–d corresponding to the regions marked on the polarization curves of Fig. 7.

Figure 8 shows the impedance diagram, which represents the open circuit potential (OCP) correlated to point (a). Figure 9 shows the impedance diagram, which represents the corrosion potential correlated to point (b). Figures 10 and 11 correlate with the potentials of passivation and transpassivation processes represented by (c) and (d), respectively.

The Ni–W–Co alloy had higher impedance values than the Co–W alloy, thus confirming the higher corrosion resistance of the former. Additionally, Figs. 8 and 9 show typical diagrams for a charge transfer process at the interface, indicating that surface reactions already occur at the OCP and corrosion potential respectively. Figure 10 shows typical diagrams for the process of passivation and dissolution that confirm the findings of the polarization curves, which suggested the presence of an unstable passive film on the surface. The same type of passivation and dissolution process was also observed by Santana et al. [14] and Keddam et al. [24]. Figure 11 shows the impedance diagrams, which can be associated with transpassivation and could be attributed to the dissolution process of the passive film. Similar behavior of impedance diagram for dissolution process was also observed by Keddam et al. [25, 26] and Bojinov et al. [27] in their studies. By the end of the impedance tests on the Co–W alloy, almost complete dissolution of the electrodeposited film occurred, exposing the surface of the copper substrate. Chemical analysis of the electrolyte of the binary alloy was done, which identified presence of copper ions in it. According to Aledresse

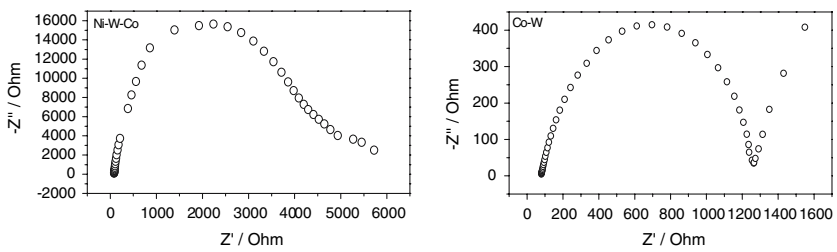

Fig. 8 Impedance diagrams related to the point (a) of the anodic polarization curves of Ni–W–Co and Co–W alloys

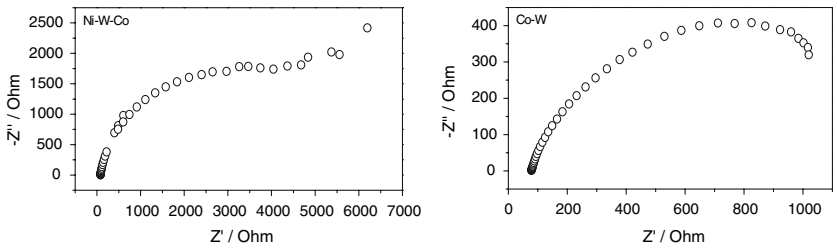

Fig. 9 Impedance diagrams related to the point (b) of the anodic polarization curves of Ni–W–Co and Co–W alloys

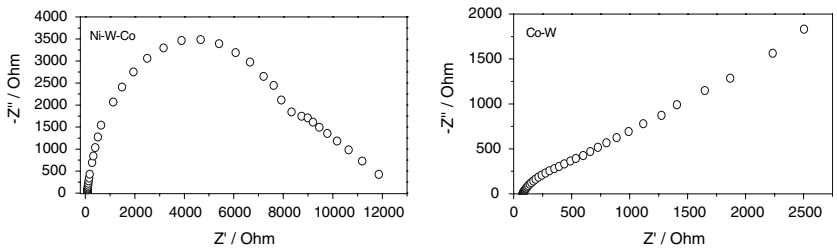

Fig. 10 Impedance diagrams related to the point (c) of the anodic polarization curves of Ni–W–Co and Co–W alloys

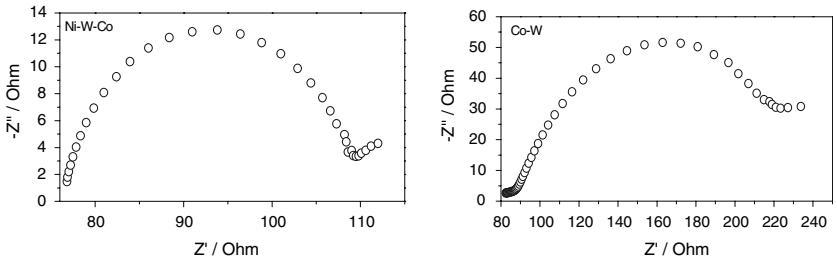

Fig. 11 Impedance diagrams related to the point (d) of the anodic polarization curves of Ni–W–Co and Co–W alloys

and Alfantazi [28], the passive film of cobalt is unstable thus favouring the high corrosion rate. In case of Ni–W–Co alloy, which was exposed to the same corrosion medium and for the same period, the copper substrate surface did not become visible. The chemical analysis of the ternary alloy electrolyte did not show presence of copper ions in the corrosion medium.

The Co–W alloy used in this study was obtained using a current density of 20 mA/cm^2, at 70 °C, with a pH of 9.5 and rotation rate at 90 rpm which gave a deposition efficiency of about 30%. The average composition of the deposit was 60 wt.% Co, 40 wt.% W with traces of boron giving a corrosion potential of –0.680 V and a polarization resistance of 1.20×10^3 Ohm.

The conditions for corrosion resistance of the Ni–W–Co alloy were a current density 60 mA/cm^2, at 70 °C, with a of pH 8.0 but with rotation rate at 20 rpm, which gave a deposition efficiency of about 36%. The average composition of the deposit was 70% Ni, 8% Co, 22% W, giving a corrosion potential of –508 V and polarization resistance of 4.56×10^4 Ohm.

Conclusions

For the optimized bath composition and within the range of operating parameters studied it can be affirmed that:

1. The ternary alloy Ni–W–Co was successfully deposited. The optimized values of operational conditions obtained, for electrodeposition of this alloy in terms of deposition efficiency, were: cathode current density 60 mA/cm^2, bath temperature 30 °C, pH 8.0 and rotation rate at 20 rpm resulting in deposition efficiency of 46%.
2. Good deposits in terms of corrosion resistance were obtained under the following operational conditions: current density 60 mA/cm^2, bath temperature 70 °C, pH 8.0 and rotation rate at 20 rpm giving a deposition efficiency of 36%.
3. The deposits obtained under optimum conditions for both deposition efficiency and corrosion resistance were of amorphous nature. These deposits showed formation of nodules, good adherence and luster.

Acknowledgement The authors are grateful to CNPq, CAPES and FINEP for financial assistance.

References

1. Younes O, Gileadi E (2003) Electrochim Acta 48:2551
2. Croopnick GA, Scrugs DM (1985) US Patent 4 529 668
3. Donten M, Stojek Z, Osteryoung JG (1993) J Electrochem Soc 140:3417
4. Habazaki H, Kawashima A, Asami K, Hashimoto K (1991) J Electrochem Soc 138:76
5. Donten M, Cesiulis H, Stojek Z (2005) Electrochim Acta 50:1405
6. Marinho FA, Santana FSM, Vasconcelos ALS, Santana RAC, Prasad S (2002) J Braz Chem Soc 13:522
7. Somekawa H, Nieh TG, Higashi K (2004) Scr Mater 50:1361
8. Eliaz N, Sridhar TM, Gileadi E (2005) Electrochim Acta 50:2893
9. Donten M (1999) J Solid State Electrochem 3:87
10. Younes O, Zhu L, Rosenberg Y, Shacham-Diamand Y, Gileadi E (2001) Langmuir 17:8270
11. Murat E (2002) Process Biochem 38:667
12. Annadurai G, Juang RS, Lee DJ (2002) Adv Inorg Environ Res 6:191
13. Singh VB, Singh LC, Tikoo PK (1980) J Electrochem Soc 127:590
14. Santana RAC, Prasad S, Campos ARN, Araújo FO, Silva GP, de Lima-Neto P (2006) J Appl Electrochem 36:105
15. Ruotolo LAM, Gubulin JC (2003) J Appl Electrochem 33:1217
16. De Faveri D, Perego P, Converti A, Del Borghi M (2002) Chem Eng J 90:291
17. Brenner A, Burkhead PS, Seegmiller E (1947) J Res Natl Bur Stand 39:351
18. Yamasaki T, Tomohira R, Ogino Y, Schloßmacher P, Ehrlich K (2000) Plat Surf Finish 87:148
19. Marinho FA, Santana FSM, Vasconcelos ALS, Santana RAC, Prasad S (2002) J Braz Chem Soc 13:522
20. Van Wonterghem J, Mørup S, Kock CJW, Charles SW, Wells S (1986) Nature 322:622
21. Qiao MH, Xie SH, Dai WL, Deng JF (2001) Catal Lett 71:187
22. Dai WL, Qiao MH, Deng JF (1997) Appl Surf Sci 120:119
23. Einati H, Bogush V, Sverdlov Y, Rosenberg Y, Shacham-Diamand Y (2005) Microelectron Eng 82:623
24. Keddam M, Mattos OR, Takenouti HJ (1981) J Electrochem Soc 128:257
25. Keddam M, Lizee JF, Pallotta C, Takenouti HJ (1984) J Electrochem Soc 131:2016
26. Keddam M, Mattos OR, Takenouti HJ (1986) Electrochim Acta 31:1147
27. Bojinov M, Betova I, Raicheff R (1998) Electrochim Acta 44:721
28. Aledresse A, Alfantazi A (2004) J Mater Sci 39:1523